ADVANCED FUNCTIONAL MATERIALS
www.afm-journal.de

Modulating Narrow Bandgap in a Diacetylene Functionalized Woven Covalent Organic Framework as a Visible Light Responsive Photocatalyst

Anahita Khojastegi, Ahmadreza Khosropour, Saeed Amirjalayer, Imann Mosleh, and Alireza Abbaspourrad**

Woven covalent organic frameworks (COF) possess entangled 3D frameworks. The metallated version of these structures contains spatially isolated Cu(I) centers and promising optoelectronic properties because of metal-to-ligand charge transfer (MLCT). However, despite their potential, woven COFs have not yet been investigated as photocatalysts. In this study, a new woven COF, Cu-PhenBDA-COF, functionalized with diacetylene bonds is developed. Cu-PhenBDA-COF is fully characterized, and the optoelectronic and photocatalytic properties are compared to previously reported Cu-COF-505. The diacetylene bonds of the linker positively impact the optoelectronic properties of Cu-PhenBDA-COF and result in a narrower bandgap and better charge separation efficiency. When the Cu(I) center is removed from both woven COFs, the absorption edge is blueshifted, resulting in a wider bandgap, and there is a considerable decrease in the charge separation efficiency, underscoring the pivotal role of MLCT. This trend is reflected in the photocatalytic activity of the woven COFs toward the degradation of sulfamethoxazole in water, where the highest reaction rate constant (k_{app}) is recorded for the metallated diacetylene functionalized woven COF, Cu-PhenBDA-COF.

1. Introduction

Photocatalysts that are designed based on reticular chemistry offer diverse synthetic modularity to adjust optical and electronic properties.[1–3] In particular, covalent organic frameworks (COFs), comprised of organic building blocks covalently bonded together, have been identified as promising photocatalysts combining tunability, crystallinity, and porosity.[1,4–6] Narrowing the bandgap of a COF photocatalyst allows the photocatalyst to harness a wider portion of the electromagnetic spectrum, especially the abundant visible light which constitutes >40% of the light generated by the sun.[4,5] To achieve this in COF-based materials, researchers typically focus on two primary approaches: functionalization and structural modification. Functionalization involves introducing electron donating or withdrawing groups to the COF structure, which can alter its electronic properties and narrow the bandgap.[7–11] Structural modification involves altering the COF structure by changing the connectivity or geometry of the COF, thus affecting the energy levels of the resulting materials' electronic states.[12–15] However, both approaches come with challenges, such as potentially destabilizing the structure of the COF or requiring complex synthetic procedures. Despite these efforts, visible light-responsive COF photocatalysts with well-separated charge carriers are still rare, and achieving this combination of properties remains a key research goal.

Woven COFs, specifically Cu-COF-505, containing woven helical organic threads and a Cu(I) center around which the threads converge and diverge, were introduced as the new generation of COFs.[16] Cu-COF-505 has many unique structural features that can be tailored for a specific application. Cu(I) serves as a point of registry, the crossing point of the organic polymer threads, and can be removed reversibly in suitable reaction conditions.[16,17] The COF-505 threads possess many degrees of freedom that allow significant deformation without affecting the structural framework.[16]

Accordingly, Cu-COF-505 has photocatalytic potential due to the inclusion of Cu(I) photosensitizers in the structure.[18] The electron-rich Cu(I) center facilitates metal-to-ligand charge transfer (MLCT) upon excitation; this extends the wavelength range of absorption.[19,20] Additionally, the unique electronic configuration of the metal center enables strong spin-orbit coupling; this promotes intersystem crossing (ISC)

A. Khojastegi, A. Khosropour, I. Mosleh, A. Abbaspourrad
Department of Food Science
College of Agriculture and Life Sciences
Cornell University
Ithaca, NY 14853, USA
E-mail: alireza@cornell.edu
S. Amirjalayer
Institute for Solid State Theory
Center for Multiscale Theory and Computation
Center for Nanotechnology
University of Münster
48149 Münster, Germany
E-mail: s.amirjalayer@uni-muenster.de
The ORCID identification number(s) for the author(s) of this article can be found under https://doi.org/10.1002/adfm.202309367

DOI: 10.1002/adfm.202309367

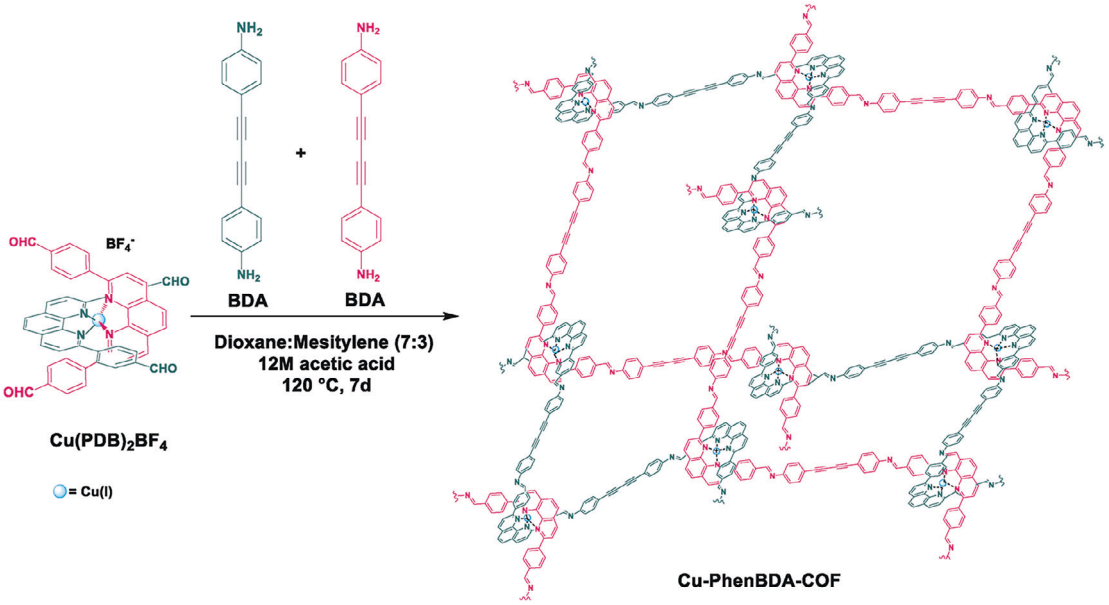

Scheme 1. The synthesis procedure of Cu-PhenBDA-COF.

between excited singlet and triplet states and improves the lifetime of the excited states and the overall photocatalytic efficiency.[18,21]

While Cu-COF-505 exhibits intriguing characteristics, further optimization could increase its range and scope of photocatalytic applications. For example, because functional groups play a key role in photocatalytic properties, fine-tuning the connectivity of the phenanthroline ligands on the metal center may enhance photocatalytic properties.[22,23] Specifically, replacing the benzidine linker with a more electron-rich linker may improve the photocatalytic properties of the woven COF. Nevertheless, constructing COFs with new functionality is challenging, and examples of woven COFs are rare.[16,17,24–27]

The inclusion of linkers with particular functional groups has improved the photocatalytic properties and tunability of the optoelectronic properties of the resulting COFs.[5] Diacetylene-bridged COFs have drawn significant interest due to their exceptionally conjugated structures, accelerated charge transfer, and accessible active sites.[28] Studies have demonstrated that COFs containing diacetylene bonds possess a narrower bandgap, facilitate intramolecular electron transfer, and enhance the delocalized electronic structure compared to their mono-acetylene counterparts or COFs lacking acetylene bonds.[28–31]

Here, we report the synthesis of a new woven COF (Cu-PhenBDA-COF) with diacetylene functionalized linkers via imine bond formation. We compared the optoelectronic properties of Cu-PhenBDA-COF with Cu-COF-505 to assess the impact of the diacetylene bond. Under appropriate reaction conditions, the Cu(I) could be removed, and we compared the optoelectronic properties of both Cu-PhenBDA-COF and Cu-COF-505 with and without the metal ion. Our new Cu-PhenBDA-COF was fully characterized, and as proof of concept, we studied its photocatalytic properties via the degradation reaction of sulfamethoxazole (SMX) in water.

2. Results and Discussion

2.1. Synthesis and Characterization of Cu-PhenBDA-COF

To synthesize the diacetylene functionalized woven COF (Cu-PhenBDA-COF), we have explored various solvent combinations and catalysts to achieve the crystalline material (Table S1, Supporting Information). Ultimately, Cu-PhenBDA-COF was synthesized by combining Cu(I)-bis[4,4′-(1,10-phenanthroline-2,9-diyl)dibenzaldehyde]tetrafluoroborate ($Cu(PDB)_2BF_4$) and 4,4′-(buta-1,3-diyne-1,4-diyl)dianiline (BDA) in a 7:3 (v/v) mixture of dioxane:mesitylene and 12 M acetic acid (**Scheme 1**).

Powder X-ray diffraction (PXRD) of Cu-PhenBDA-COF confirmed its high crystallinity and periodic structure (**Figure 1b**). To characterize the atomistic structure in detail, we modeled the framework at the atomic level using a molecular mechanics approach. In this context, we extended the MM3 force field[32–34] to describe the Cu(I) environment using our previously introduced genetic algorithm-based parametrization protocol.[35–37] We used a united-atom representation for the counter anion together with a simplified charge representation (Cu: +1 and ion: −1). The structure was explored based on this force field and starting from the reported Cu-COF-505 network topology, and the simulated XRD patterns were compared with the experimental data. The framework structure, which is constructed by an interpenetration of two mesh structures (Figure 1a,c), is in good agreement with the experimental pattern. The Cu-PhenBDA-COF (cell parameters: a = 25.46; b = 15.50; c = 39.79; α = 85.02; β = 92.32; γ = 90.13 Å) thus contains a similar network, iso-reticular, as the Cu-COF-505 structure (Table S2, Supporting Information).

Fourier transform infrared (FTIR) spectroscopy was used to assess the presence, or absence, of key functional groups in the structure of Cu-PhenBDA-COF (**Figure 2a**). The disappearance of the C═O stretching vibration of the aldehyde groups at 1695 cm^{-1} and the N—H stretching vibration frequency at 3400 cm^{-1}

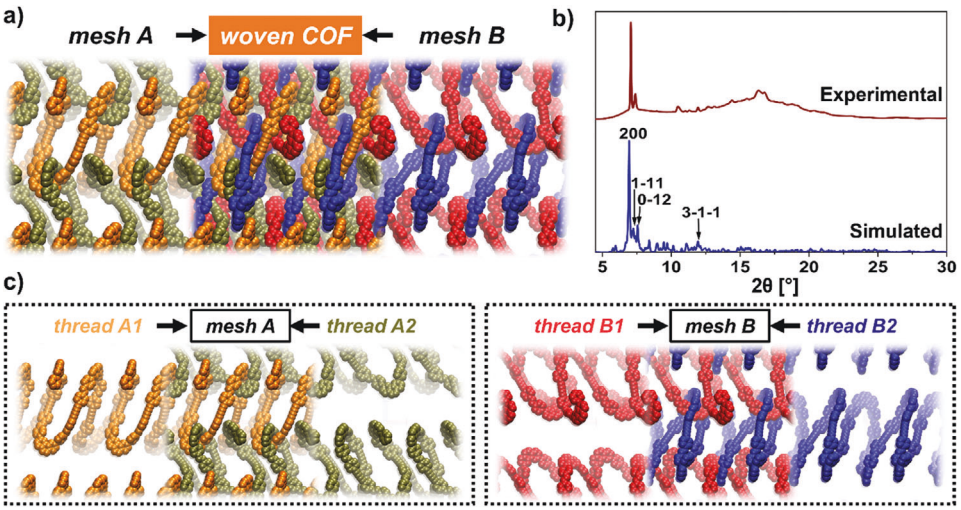

Figure 1. a) Periodic structure of the Cu-PhenBDA-COF derived from the molecular mechanics investigations (for clarity, the individual threads are color-coded, and the free ions are removed). b) Comparison of the experimentally measured synchrotron PXRD and simulated PXRD patterns (blue). c) Atomistic structure of the Cu-PhenBDA-COF decomposed into the respective threads and mesh forming the crystalline structure.

(corresponding to the primary amine group), and the appearance of a new band at 1622 cm^{-1} pertaining to a C═N stretching vibration of an imine bond provides evidence of the complete conversion of the aldehyde and amine groups to the corresponding imine bond.[17,38,39]

The CPMAS solid-state ^{13}C NMR spectrum of Cu-PhenBDA-COF (Figure 2b) shows multiple peaks from 140 to 160 ppm; these chemical shifts are typical of C═N double bonds. The disappearance of the aldehyde group of $Cu(PDB)_2BF_4$ at 190 ppm indicates the high polymerization degree of this COF.[16,40] The acetylenic carbons appear at 70 and 80 ppm, confirming that the functionality of the linkers has not changed during synthesis. (Detailed NMR assignments are provided in Figure S1, Supporting Information.)

The SEM images of Cu-PhenBDA-COF showed spherical morphology with a diameter of 1.5–2.5 µm, similar to that of Cu-COF-505 (**Figure 3**a,b). The TEM images (Figure 3d,e) also confirmed the spherical morphology of the Cu-PhenBDA-COF and its woven structure where the weave is highlighted with the dark and light crossings of the warp (the dark lines) and weft (the white lines moving up and down).

The XPS spectra of Cu-PhenBDA-COF showed the presence of Cu, F, N, and C, confirming the preservation of the Cu(I) complex and the BF_4^- counterion (Figure 3c). The C 1s spectra were deconvoluted to several peaks centered around binding energies of 283.0, 284.4, 284.9, 285.5, and 286.5 eV, corresponding to C═C, C≡C, C═N phenanthroline, C═N imine, and the satellite peak, respectively (Figure 3f). Similarly, the deconvoluted N 1s spectra showed two peaks; one peak is centered at 397.4 eV and correlates to the C═N imine, while the other at 399.0 eV is related to C═N phenanthroline (Figure S2a, Supporting Information). The Cu 2p spectra confirmed the presence and purity of Cu(I) in the system (Figure S2b, Supporting Information).

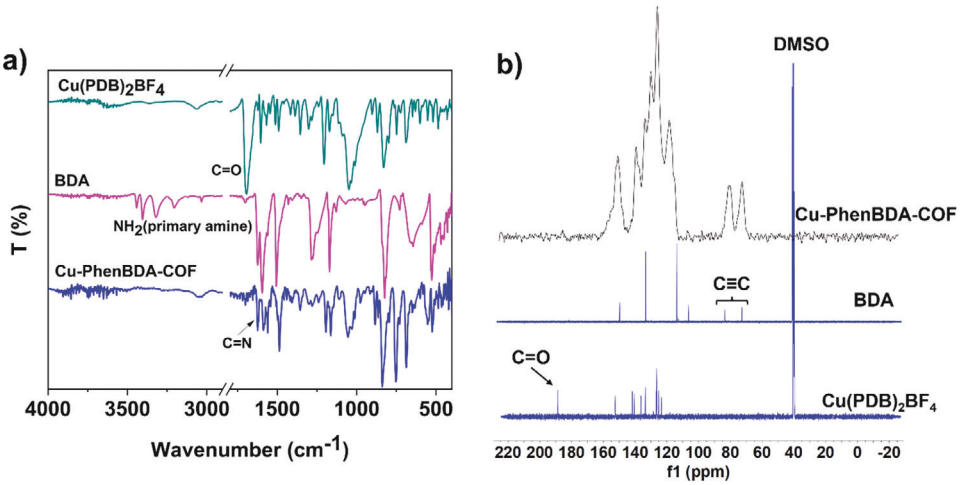

Figure 2. a) FTIR spectra, and b) CPMAS solid-state ^{13}C NMR spectra of Cu-PhenBDA-COF, BDA, and $Cu(PDB)_2BF_4$ in DMSO-d_6.

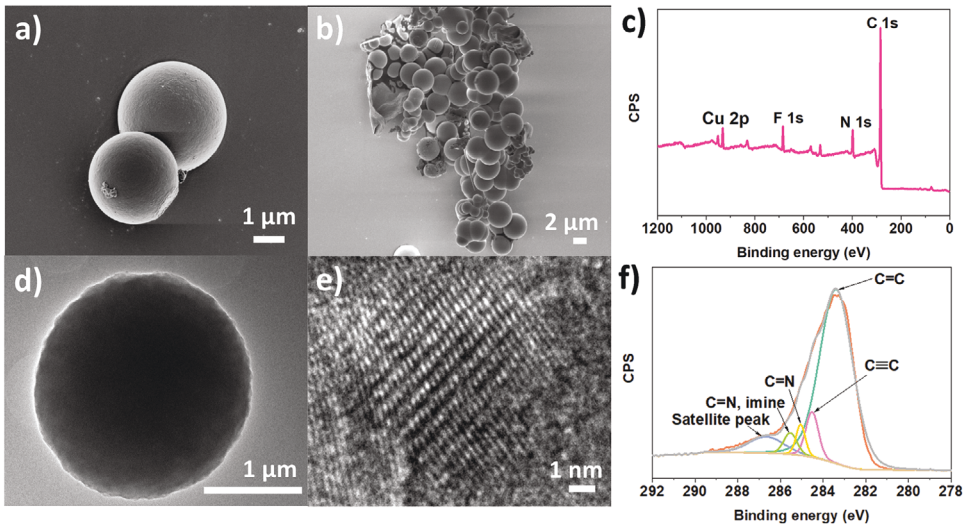

Figure 3. a,b) SEM images, d,e) HR-TEM images, c) XPS survey spectra, and f) C 1s XPS high-resolution spectra of Cu-PhenBDA-COF.

The thermal stability of Cu-PhenBDA-COF was assessed using thermogravimetric analysis (TGA) and showed the excellent thermal stability of the structure up to 400°C (Figure S3, Supporting Information). The major weight loss occurred above 400 °C, accounting for 28% of the sample weight arising from the carbonization of the sample in the nitrogen atmosphere.

We also synthesized Cu-COF-505 to compare the optoelectronic and photocatalytic activity to Cu-PhenBDA-COF (Scheme S1, Supporting Information). The PXRD of the as-synthesized Cu-COF-505 matched those reported. (Figure S4a, Supporting Information).[16] We also removed Cu(I) from the structure of Cu-PhenBDA-COF and Cu-COF-505 post-synthetically to compare the optoelectronic and photocatalytic activity to the metallated counterpart (Schemes S1 and S2, Supporting Information). The demetallation of the woven COFs was confirmed by nitric acid-digested samples using inductively coupled plasma mass spectrometry (ICP-MS), and the results showed that 94.1 ± 3.1% and 95.0 ± 2.6% of Cu(I) were removed from Cu-PhenBDA-COF and Cu-COF-505, respectively. Further, upon demetallation, we observed that when Cu(I) was removed from the COF structure, the dark red-brown colors of the Cu-COFs, arising from MLCT, changed to pale yellow. The PXRD of the demetallated woven COFs (Figure S4, Supporting Information) showed a reduction in the peak intensity, arising from the increased flexibility of the woven COF.[16]

2.2. Optoelectronic Properties of the Woven COFs

Diffuse reflectance ultraviolet–visible spectroscopy (DRS-UV–vis) was performed to evaluate the light-harvesting properties of woven COFs.[16] For Cu-COF-505 the absorption edge is ≈550 nm, while Cu-PhenBDA-COF showed a broad absorption covering almost the entire visible-light region, the absorption edge is estimated to be 650 nm with a tail that continued to 800 nm (**Figure** 4a). These results indicate the positive impact of the diacetylene bond in the light-harvesting ability of Cu-PhenBDA-COF compared to Cu-COF-505. The absorption edge of the demetallated COFs, PhenBDA-COF and COF-505, is blueshifted to 450 nm, indicating the importance of metal in the structure of woven COF and the role of MLCT in visible light absorption.

The optical bandgaps of the woven COFs calculated from the Tauc plot[41] were found to be 1.86 and 2.05 eV for Cu-PhenBDA-COF and Cu-COF-505, respectively, while for the demetallated woven COFs the bandgaps were wider with 2.31 eV for PhenBDA-COF and 2.47 eV for COF-505 (Figure S5, Supporting Information). These observations indicate the importance of both the diacetylene groups on the linker, as well as the Cu(I), to improve the light-harvesting properties of the Cu-PhenBDA-COF and narrow the bandgap compared to Cu-COF-505.

To gain more insight into the electronic properties of the woven COFs, the highest occupied molecular orbital (HOMO) and lowest unoccupied molecular orbital (LUMO) energy levels were estimated using different methods (Figure 4b). Mott–Schottky plots of woven COFs displayed the negative slopes, typical of n-type semiconductors (Figure S6, Supporting Information). For n-type semiconductors, the flat band potentials are usually close to the LUMO and thus were estimated to be −0.63, −0.49, −0.19, and −0.17 V versus normal hydrogen electrode (NHE) for Cu-PhenBDA-COF, Cu-COF-505, PhenBDA-COF, and COF-505, respectively.[42,43] Cyclic voltammetry (CV) was used to estimate the HOMO level, and the onset of the oxidation potential of woven COFs indicates the HOMO to be 1.15, 1.45, 2.04, and 2.17 V versus NHE for Cu-PhenBDA-COF, Cu-COF-505, PhenBDA-COF, and COF-505, respectively (Figure S7, Supporting Information).[44,45] Our experimentally observed spectroscopic measurements and electrochemical measurements, are in good agreement with the calculated estimated bandgap for our woven COFs.

Ultraviolet photoelectron spectroscopy (UPS) was also used to estimate the energy level of the HOMOs of Cu-PhenBDA-COF and Cu-COF-505 (Figure S8, Supporting Information). The HOMO level versus vacuum for Cu-PhenBDA-COF was found at 5.94 eV, while for Cu-COF-505 it was 6.27 eV, which is in good agreement with our electrochemical measurements. These

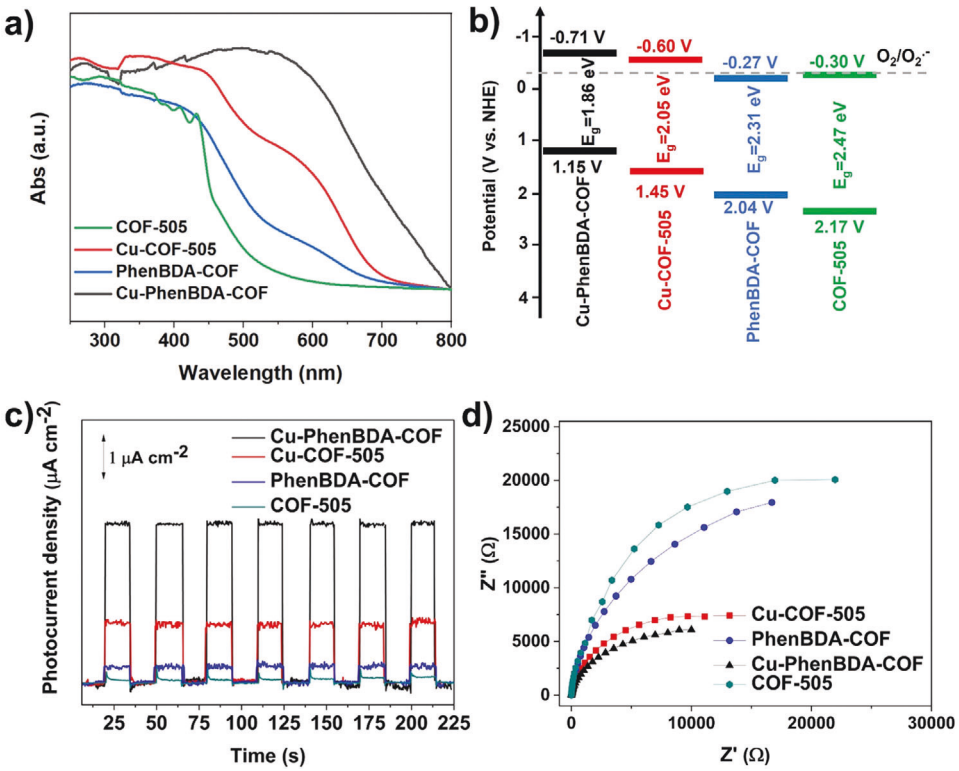

Figure 4. a) DRS-UV–vis spectra of woven COFs. b) The energy band structure of woven COFs. c) Transient photocurrent measurements of woven COFs. d) Nyquist plot of woven COFs in light.

results show that the LUMO energy levels of metallated woven COFs are well-positioned and thermodynamically suitable for producing radicals by oxygen reduction.

We conducted transient photocurrent measurements to examine the separation and movement of electron-hole pairs generated by light; Cu-PhenBDA-COF showed a higher photocurrent response than Cu-COF-505 (Figure 4c). The low photocurrent response for Cu-COF-505 is due to the C—C single bond linking the two benzene rings, which may result in the partial destruction of charge dislocation.[28–30] Conversely, the diacetylene bond in Cu-PhenBDA-COF can promote a coplanar conformation favorable for charge separation.[28–30] A higher photocurrent response was recorded for the metallated woven COFs compared to the demetallated ones indicating the role of the metal in the charge separation of photogenerated charge carriers.

Electrochemical impedance spectroscopy (EIS) confirmed the photocurrent responses (Figure 4d). The smaller semicircles associated with the metallated woven COFs compared to the demetallated counterparts indicate the lower charge transfer resistance of the metallated COFs which we attribute to the presence of the Cu(I) ion.

In addition, density functional theory (DFT) calculations at the CAM-B3LYP/SDD[46–48] level were performed at non-periodic model systems to identify the relevant electronic transitions induced by light excitation. These calculations show a metal-to-ligand excitation for both Cu-COF-505 and Cu-PhenBDA-COF (**Figure 5**). However, detailed analysis revealed that in the case of Cu-PhenBDA-COF, the excitation from the metal center to the organic ligands is promoted due to the coupling of the diacetylene ligand with the metal-centered orbitals. This is reflected by an increase of the calculated oscillator strength *f* for the first two metal to ligand electronic excitations going from 0.0519 to 0.0867 and from 0.0964 to 0.1791, respectively (Figure 5). The enhanced MLCT indicates a significant change in the light absorption properties.

2.3. Photocatalytic Properties of the Woven COFs

We evaluated the photocatalytic properties of Cu-PhenBDA-COF in the photocatalytic degradation of sulfamethoxazole (SMX) in water. SMX, one of the top ten prescribed antibiotics for humans, livestock, and aquaculture worldwide, is frequently detected in natural water due to its stability toward biodegradation.[49,50] The degradation rate of SMX using Cu-PhenBDA-COF as a photocatalytic system follows a pseudo-first-order kinetic model $ln\frac{C_t}{C_0} = -k_{app}t$, where C_t and C_0 correspond to the concentration of SMX at time *t*, and 0 min and k_{app} are the apparent pseudo-first-order rate constant. We observed that Cu-PhenBDA-COF can adsorb ≈10% of SMX under dark conditions. Under white LED light conditions, Cu-PhenBDA-COF degraded 99.9% of the SMX in 100 min, and the reaction rate constant (k_{app}) was found to be 0.0467 min^{-1}. Cu-COF-505 also adsorbed ≈10% of the SMX under similar dark conditions; however, under light conditions, 50% of the SMX was degraded within the same time frame (**Figure 6**a). The k_{app} for Cu-COF-505 was found to be 0.0079 min^{-1} (Figure S9, Supporting Information). Without a catalyst, SMX did not degrade within the 100 min time frame. We attribute the

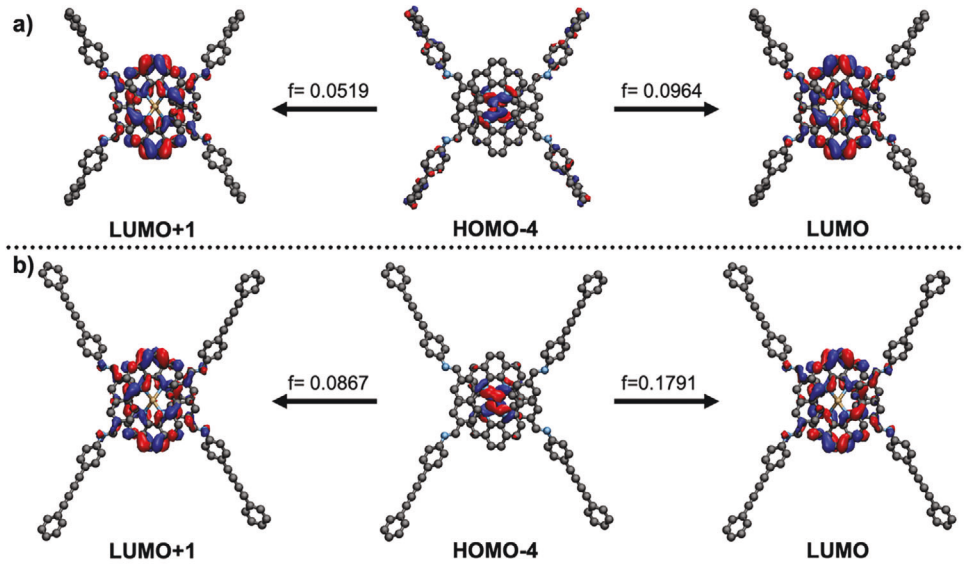

Figure 5. Molecular orbitals representing the two metals to ligand electronic excitation (left and right) of the a) Cu-COF-505, and b) Cu-PhenBDA-COF calculated at the CAM-B3LYP/SDD//B3LYP/SDD level for non-periodic model systems together with the corresponding oscillator strength *f*. Hydrogen atoms are omitted for clarity.

superior performance of Cu-PhenBDA-COF over Cu-COF-505 to the presence of the diacetylene bond that endows Cu-PhenBDA-COF with better light-harvesting properties, charge separation efficiency and thus, vastly better photocatalytic activity.

Additionally, the $Cu(PDB)_2BF_4^-$complex removed <20% of SMX in the first 20 min of the reaction, and after that no further degradation was detected. These results imply that the superior photocatalytic properties of Cu-PhenBDA-COF compared to other COFs stem from its optoelectronic properties.

We also investigated the photocatalytic degradation of SMX using the demetallated COFs (PhenBDA-COF and COF-505). Our results showed that the demetallated COFs had inferior photocatalytic properties compared to the metallated counterparts, with <10% of the SMX degraded within 100 min. This lower degradation rate compared to the metallated COFs could be associated with the role of Cu(I) in the structure. To optimize the photocatalytic performance of Cu-PhenBDA-COF, we examined the effects of pH, photocatalyst dosage, and initial concentration on the degradation of SMX. First, the influence of the photocatalyst dosage in the photocatalytic degradation of SMX was evaluated. As shown in Figure 6b, increasing the amount of Cu-PhenBDA-COF from 100 to 400 mg L^{-1} considerably increased the k_{app} from 0.0106 to 0.0467 min^{-1} (Figure S10a, Supporting Information). At a dosage of 100 mg L^{-1}, Cu-PhenBDA-COF can degrade 65.9% of the SMX within 100 min, while 400 mg L^{-1} of Cu-PhenBDA-COF reached 99.9% of SMX degradation within 100 min. These results indicate that when more COF is used, more active sites are present for light absorption, and more reactive oxygen species (ROS) are produced; more ROS leads to faster degradation of SMX. However, when the catalyst dosage was increased to 600 mg L^{-1}, a sharp decrease was observed in $k_{app,}$ (0.0269 min^{-1}) compared to 400 mg L^{-1}, which can be attributed to inefficient light harvesting due to the blockage of the light pathway by the COF particles suspended in the solution. As such, 400 mg L^{-1} Cu-PhenBDA-COF was selected as the optimum concentration of the COF at pH 7, and an SMX concentration of 5 mg L^{-1} since the highest k_{app} (0.0467 min^{-1}) was recorded at this concentration.

The effect of the initial concentration of SMX with the optimum amount of the COF photocatalyst (400 mg L^{-1}) on SMX degradation was also assessed (Figure 6c). We observed that as the SMX concentration increased, the removal percentage by the adsorption in the dark decreased from 10.1% at 5 mg L^{-1} to 6.0% at 15 mg L^{-1}. In light, a decreasing trend was also observed in the k_{app} of SMX degradation, as the SMX initial concentration increased from 5 to 10 to 15 mg L^{-1}, k_{app} was found to be 0.0467, 0.0234, and 0.0180 min^{-1}, respectively (Figure S10b, Supporting Information). With higher concentrations of SMX, more ROS is required for degradation, and at the optimum concentration of COF, it takes longer to produce ROS, thus the degradation kinetics slows down.

Considering the pH dependency of SMX, we also studied the degradation efficiency of SMX at different pH levels (Figure S11, Supporting Information).[40] In the dark, the adsorption of SMX on the surface of Cu-PhenBDA-COF in acidic pH was higher than in neutral or basic pH. This adsorption trend correlates to the different surface charges of the COF, which has a zero-point charge at pH 5.8. This means that at lower pH levels the positively charged surface of Cu-PhenBDA-COF would have greater electrostatic interactions with neutral SMX; however, once the pH increases to 7 and 9, the surface of the COF is negatively charged, but the SMX also bears negative charges resulting in electrostatic repulsion and decreased adsorption (Figure S11a, Supporting Information).[51] In light, degradation of SMX improved when the pH increased from 3 to 9 and k_{app} increased from 0.0115 to 0.0622 min^{-1}, respectively. The slower degradation rate at acidic pH levels can be attributed to the radical scavenger properties of hydronium ions. However, once the pH level increases, the hydroxyl ions can facilitate the production of ROS in the reaction, resulting in degradation rate acceleration.

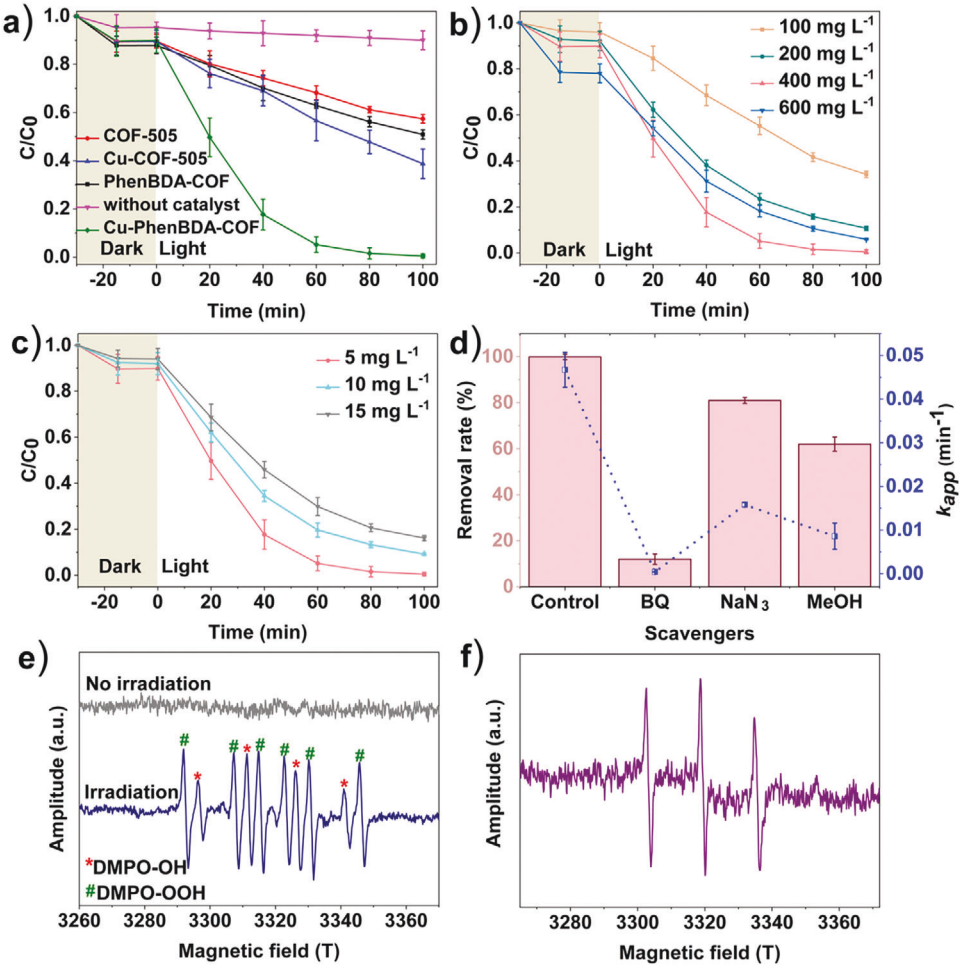

Figure 6. The decomposition of SMX with a) different photocatalysts [SMX] = 5 mg L^{-1}, [Catalyst] = 400 mg L^{-1}, pH 7. b) different photocatalyst dosages [SMX] = 5 mg L^{-1}, pH 7. c) different SMX concentrations [Catalyst] = 400 mg L^{-1}, pH 7. d) Removal efficiency of different radical scavengers. e) EPR measurements using DMPO. f) EPR measurements using TEMPO.

The reusability of Cu-PhenBDA-COF in photocatalytic degradation of SMX in three consecutive runs was evaluated (Figure S12, Supporting Information). SMX removal efficiencies over three cycles were 99.9%, 97.9%, and 94.1% within 100 min of the reaction. The PXRD and FTIR spectra of recycled Cu-PhenBDA-COF after three runs showed only slight changes compared to the fresh catalyst, confirming the stability and reusability of this catalyst under our experimental conditions (Figure S13, Supporting Information).

To determine the nature of the ROS produced in the photocatalytic degradation of SMX, we used different radical scavengers to investigate the inhibition effect on the reaction rate constant (Figure 6d).[49] We started with methanol (MeOH), a scavenger for hydroxyl radical (•OH) with a known rate constant of $k = 9.7 \times 10^8$ mol^{-1} s^{-1}. The experiment with 200 mM MeOH showed 35% inhibition of the degradation rate of SMX compared to the control, suggesting the possible role of •OH. Next, benzoquinone (BQ) and NaN_3 were used to investigate the possible role of superoxide radical ($O_2^{\bullet -}$) ($k = 3.2 \times 10^7$ mol^{-1} s^{-1}) and singlet oxygen ($^1O_2$) ($k = 1.0 \times 10^9$ mol^{-1} s^{-1}) in the degradation of SMX, respectively. In our experimental condition, the presence of NaN_3 decreased the removal efficiency to ≈78%, and BQ only removed almost 19% of SMX in the reaction rate. These results illustrated that $O_2^{\bullet -}$ is possibly the main ROS involved in the photocatalytic degradation of SMX using Cu-PhenBDA-COF.

To validate the quenching experiment results, we used Electron Paramagnetic Resonance (EPR) spectroscopy using the spin-trapping technique. 5,5-Dimethyl-1-pyrroline-*N*-oxide (DMPO) and 2,2,6,6-tetramethylpiperidine-*N*-oxide (TEMPO) were used as spin-trapping agents (Figure 6e,f). In the presence of DMPO a ten-line signal can be observed when the system is irradiated. This observation can be attributed to two distinguishable radicals: •OH and $O_2^{\bullet -}$. The four-fold signals (marked with red stars) with an intensity ratio of 1:2:2:1 (hyperfine splitting constants: a_N = 14.72 G) were assigned to DMPO-OH adduct, while the six lined signals were attributed to DMPO-OOH adduct.[52] The detection of DMPO-OH and DMPO-OOH adducts confirms the presence of •OH and $O_2^{\bullet -}$ in our photocatalytic system. When TEMPO was used as the spin trapping agent, a threefold signal with a ratio of 1:1:1 adduct and a hyperfine splitting constant a_N = 16.87 G characteristic of a TEMPO-$^1O_2$ confirmed the presence of $O_2^{\bullet -}$.[53]

Finally, the intermediates in the photocatalytic degradation of SMX were investigated by LC-MS using an aliquot collected at ≈30 min of reaction time under optimized conditions. We proposed two pathways that could be involved in the degradation of SMX (*m/z* 254) based on the detected masses and literature, including i) oxidation and ii) bond cleavage, as illustrated in Scheme S3 (Supporting Information).[50,54,55] The benzene ring was easily hydroxylated by active •OH to form an oxidation product with *m/z* 270, and oxidation of the —CH_3 group or —NH_2 group resulted in an oxidation product with *m/z* 284, while the masses with *m/z* 174, 109, 99 are the C—S and N—S bond cleavage intermediates of SMX (Figure S15, Supporting Information).[49] Conversely, no degradation product was detected under dark conditions or when the Cu-PhenBDA-COF was not present in an illuminated SMX sample (Figures S16 and S17, Supporting Information). These results indicate that our photocatalytic system is highly efficient in harvesting visible light and the generation of radicals.

3. Conclusion

In summary, we synthesized and characterized Cu-PhenBDA-COF as a novel diacetylene functionalized woven COF, that is catalytically active under visible light producing ROS suitable for the degradation of SMX. We compared the optoelectronic properties of Cu-PhenBDA-COF with Cu-COF-505; we observed that incorporating a diacetylene bond improved the light-harvesting properties in the visible region by >100 nm and narrowed the optical bandgap by >10% from 2.05 eV for Cu-COF-505 to 1.86 eV for our Cu-PhenBDA-COF. Our results showed that the Cu(I) metal center plays a crucial role in the light adsorption properties of the woven COFs through an MLCT mechanism. The photocatalytic properties of these COFs were evaluated for the degradation of SMX in water. It was found that Cu-PhenBDA-COF possessed the highest photocatalytic activity and that 99.9% of the SMX is degraded after 100 min under visible light irradiation. The degradation pathway was investigated with LC-MS, and two major pathways of oxidation and bond cleavage were proposed. The ROS produced in our photocatalytic system was determined, and our data suggest the presence of $O_2^{\bullet -}$ plays a major role in the photocatalytic degradation of SMX. To the best of our knowledge, this is the first study on the optoelectronic and photocatalytic properties of woven COFs, and we believe that this examination can open a new avenue for designing and developing new photocatalysts based on these types of materials.

4. Experimental Section

Synthesis and Activation of COF-505: COF-505 was synthesized based on a previously reported procedure.[16]

Synthesis and Activation of Cu-PhenBDA-COF: $Cu(PDB)_2BF_4$ (15 mg, 0.016 mmol), BDA (8.0 mg, 0.032 mmol), and 1 mL of an anhydrous mixture of mesitylene:dioxane (3:7) were placed in a Pyrex tube. Subsequently, 100 µL of acetic acid (12 M) was added to the mixture. The tube was degassed via freeze-pump-thaw method using a liquid N_2 bath and a vacuum pump. After degassing, the tube was sealed and placed in an oven at 120 °C for 7 d. After cooling, the glass tubes were cut, and the contents were filtered. The dark reddish-brown solid was collected, washed with DMF, and then, using Soxhlet apparatus, washed with THF for 24 h. The sample (15 mg) was then dried at 60 °C in a vacuum oven for 12 h. (Elemental analysis calculated for $C_{84}H_{48}BCuF_4N_8.4H_2O$: C, 75.08%, H, 4.20%, N, 8.34%, Cu, 4.73%, Found: C, 69.86%, H, 3.99%, N, 7.88%, Cu, 5.30% (Cu % based on ICP-MS)).

Photocatalytic Degradation of SMX: Photocatalytic experiments were performed at room temperature in a 125 mL cubic quartz reactor using a homemade light box equipped with four high-power white LED lamps (179 lm W^{-1}). As the optimum reaction condition, we first dispersed 20 mg of the COF in 50 mL of a 5 mg L^{-1} solution of SMX. The mixture was stirred for 30 min to reach the adsorption–desorption equilibrium. The degradation reaction was initiated by turning on the light. At predetermined time intervals, 0.5 mL of the mixture was withdrawn and filtered, and the concentration of SMX over time was measured using a SHIMADZU UV–vis spectrophotometer at 257 nm.

The degradation intermediates of SMX were determined using a Thermo Q Exactive ion trap mass spectrometer equipped with liquid chromatography. A reversed-phase C18 (Luna Phenomenex 4.6 × 100 mm, 5 µM) column was used for separation at room temperature.

Supporting Information

Supporting Information is available from the Wiley Online Library or from the author.

Acknowledgements

This study utilized shared facilities of the Cornell Center for Materials Research sponsored through the NSF MRSEC program (DMR-1719875). This work made use of the ACERT center facilities at Cornell University, NIH/NIGMS ACERT center grant P41GM103521. This work also made use of the Cornell University NMR Facility, which is supported, in part, by the NSF through MRI award CHE1531632. The computations were done using the resources of PALMA@WWU. This work is based on research conducted at the Center for High-Energy X-ray Sciences (CHEXS), which is supported by the National Science Foundation (BIO, ENG, and MPS Directorates) under award DMR-1829070., and the Macromolecular Diffraction at CHESS (MacCHESS) facility, which is supported by award 1-P30-GM124166-01A1 from the National Institute of General Medical Sciences, National Institutes of Health, and by New York State's Empire State Development Corporation (NYSTAR).

Conflict of Interest

The authors declare no conflict of interest.

Author Contributions

A.K. performed conceptualization, investigation, designing of methodology, and data curation, wrote the original draft, and wrote, edited, and reviewed the manuscript; A.K. performed conceptualization and investigation, wrote, edited, and reviewed the manuscript; S.A. wrote, edited, and reviewed the manuscript, and conceived and performed the atomistic simulations; I.M. performed investigation and wrote, edited, and reviewed the manuscript; A.A. performed conceptualization, funding acquisition, project administration, resources acquisition, and supervision, and wrote, edited, and reviewed the manuscript.

Data Availability Statement

The data that support the findings of this study are available from the corresponding author upon reasonable request.

Keywords

metal-to-ligand charge transfer, narrow bandgap, photocatalysis, water treatment, woven covelant organic frameworks

Received: August 8, 2023
Revised: October 11, 2023
Published online: December 2, 2023

[1] Q. Yang, M. Luo, K. Liu, H. Cao, H. Yan, *Appl. Catal. B* **2020**, *276*, 119174.
[2] Y. Qian, F. Zhang, H. Pang, *Adv. Funct. Mater.* **2021**, *31*, 2104231.
[3] O. M. Yaghi, M. J. Kalmutzki, C. S. Diercks, *Introduction to Reticular Chemistry: Metal-Organic Frameworks and Covalent Organic Frameworks*, John Wiley & Sons, Hoboken, NJ, USA **2019**.
[4] H. Wang, H. Wang, Z. Wang, L. Tang, G. Zeng, P. Xu, M. Chen, T. Xiong, C. Zhou, X. Li, D. Huang, Y. Zhu, Z. Wang, J. Tang, *Chem. Soc. Rev.* **2020**, *49*, 4135.
[5] R. Liu, K. T. Tan, Y. Gong, Y. Chen, Z. Li, S. Xie, T. He, Z. Lu, H. Yang, D. Jiang, *Chem. Soc. Rev.* **2021**, *50*, 120.
[6] C. Cavedon, S. Gisbertz, S. Reischauer, S. Vogl, E. Sperlich, J. H. Burke, R. F. Wallick, S. Schrottke, W.-H. Hsu, L. Anghileri, Y. Pfeifer, N. Richter, C. Teutloff, H. Müller-Werkmeister, D. Cambié, P. H. Seeberger, J. Vura-Weis, R. M. Van Der Veen, A. Thomas, B. Pieber, *Angew. Chem., Int. Ed. Engl.* **2022**, *61*, 202211433.
[7] J. Wang, W. Zhu, F. Meng, G. Bai, Q. Zhang, X. Lan, *ACS Catal.* **2023**, *13*, 4316.
[8] Y. Zhang, L. Cao, G. Bai, X. Lan, *Small* **2023**, *19*, e2300035.
[9] J.-N. Chang, J.-W. Shi, Q. Li, S. Li, Y.-R. Wang, Y. Chen, F. Yu, S.-L. Li, Y.-Q. Lan, *Angew. Chem. Int. Ed. Engl.* **2023**, *62*, e202303606.
[10] W. Chen, L. Wang, D. Mo, F. He, Z. Wen, X. Wu, H. Xu, L. Chen, *Angew. Chem. Int. Ed. Engl.* **2020**, *59*, 16902.
[11] S. Li, L. Li, Y. Li, L. Dai, C. Liu, Y. Liu, J. Li, J. Lv, P. Li, B. Wang, *ACS Catal.* **2020**, *10*, 8717.
[12] P. Das, G. Chakraborty, J. Roeser, S. Vogl, J. Rabeah, A. Thomas, *J. Am. Chem. Soc.* **2023**, *145*, 2975.
[13] Y. Meng, Y. Luo, J.-L. Shi, H. Ding, X. Lang, W. Chen, A. Zheng, J. Sun, C. Wang, *Angew. Chem., Int. Ed. Engl.* **2020**, *59*, 3624.
[14] C. Wu, Z. Teng, C. Yang, F. Chen, H. B. Yang, L. Wang, H. Xu, B. Liu, G. Zheng, Q. Han, *Adv. Mater.* **2022**, *34*, 2110266.
[15] J. Xu, C. Yang, S. Bi, W. Wang, Y. He, D. Wu, Q. Liang, X. Wang, F. Zhang, *Angew. Chem. Int. Ed. Engl.* **2020**, *59*, 23845.
[16] Y. Liu, Y. Ma, Y. Zhao, X. Sun, F. Gándara, H. Furukawa, Z. Liu, H. Zhu, C. Zhu, K. Suenaga, P. Oleynikov, A. S. Alshammari, X. Zhang, O. Terasaki, O. M. Yaghi, *Science* **2016**, *351*, 365.
[17] Y. Liu, Y. Ma, J. Yang, C. S. Diercks, N. Tamura, F. Jin, O. M. Yaghi, *J. Am. Chem. Soc.* **2018**, *140*, 16015.
[18] K. Chen, L. Yang, Z. Wu, C. Chen, J. Jiang, G. Zhang, *Phys. Chem. Chem. Phys.* **2019**, *21*, 546.
[19] R. Czerwieniec, M. J. Leitl, H. H. H. Homeier, H. Yersin, *Coord. Chem. Rev.* **2016**, *325*, 2.
[20] N. Armaroli, *Chem. Soc. Rev.* **2001**, *30*, 113.
[21] J. Zhao, W. Wu, J. Sun, S. Guo, *Chem. Soc. Rev.* **2013**, *42*, 5323.
[22] Y. Sun, Z. M. Hudson, Y. Rao, S. Wang, *Inorg. Chem.* **2011**, *50*, 3373.
[23] M. R. Waterland, A. Flood, K. C. Gordon, *J. Chem. Soc. Dalton Trans.* **2000**, *0*, 121.
[24] H.-S. Xu, Y. Luo, X. Li, P. Z. See, Z. Chen, T. Ma, L. Liang, K. Leng, I. Abdelwahab, L. Wang, R. Li, X. Shi, Y. Zhou, X. F. Lu, X. Zhao, C. Liu, J. Sun, K. P. Loh, *Nat. Commun.* **2020**, *11*, 1434.
[25] H.-S. Xu, Y. Luo, P. Z. See, X. Li, Z. Chen, Y. Zhou, X. Zhao, K. Leng, I.-H. Park, R. Li, C. Liu, F. Chen, S. Xi, J. Sun, K. P. Loh, *Angew. Chem., Int. Ed. Engl.* **2020**, *59*, 11527.
[26] Y. Liu, C. S. Diercks, Y. Ma, H. Lyu, C. Zhu, S. A. Alshmimri, S. Alshihri, O. M. Yaghi, *J. Am. Chem. Soc.* **2019**, *141*, 677.
[27] X. Kang, X. Wu, X. Han, C. Yuan, Y. Liu, Y. Cui, *Chem. Sci.* **2019**, *11*, 1494.
[28] L. Chen, L. Wang, Y. Wan, Y. Zhang, Z. Qi, X. Wu, H. Xu, *Adv. Mater.* **2020**, *32*, 1904433.
[29] P. Pachfule, A. Acharjya, J. Roeser, T. Langenhahn, M. Schwarze, R. Schomäcker, A. Thomas, J. Schmidt, *J. Am. Chem. Soc.* **2018**, *140*, 1423.
[30] S. Thomas, H. Li, R. R. Dasari, A. M. Evans, I. Castano, T. G. Allen, O. G. Reid, G. Rumbles, W. R. Dichtel, N. C. Gianneschi, S. R. Marder, V. Coropceanu, J.-L. Brédas, *Mater. Horiz.* **2019**, *6*, 1868.
[31] X. Lan, X. Liu, Y. Zhang, Q. Li, J. Wang, Q. Zhang, G. Bai, *ACS Catal.* **2021**, *11*, 7429.
[32] N. L. Allinger, Y. H. Yuh, J. H. Lii, *J. Am. Chem. Soc.* **1989**, *111*, 8551.
[33] N. L. Allinger, F. Li, L. Yan, J. C. Tai, *J. Comput. Chem.* **1990**, *11*, 868.
[34] C. E. Kundrot, J. W. Ponder, F. M. Richards, *J. Comput. Chem.* **1991**, *12*, 402.
[35] S. Amirjalayer, R. Schmid, *J. Phys. Chem. C* **2016**, *120*, 27319.
[36] E. Kolodzeiski, S. Amirjalayer, *J. Chem. Theory Comput.* **2021**, *17*, 7010.
[37] E. Kolodzeiski, S. Amirjalayer, *Sci. Adv.* **2022**, *8*, eabn4426.
[38] R. Javad Kalbasi, A. Khojastegi, *Catal Lett.* **2018**, *148*, 958.
[39] Y. Liu, J. Li, J. Lv, Z. Wang, J. Suo, J. Ren, J. Liu, D. Liu, Y. Wang, V. Valtchev, S. Qiu, D. Zhang, Q. Fang, *J. Am. Chem. Soc.* **2023**, *145*, 9679.
[40] D. Abdullatif, A. Khosropour, A. Khojastegi, I. Mosleh, L. Khazdooz, A. Zarei, A. Abbaspourrad, *ACS Appl. Polym. Mater.* **2023**, *5*, 412.
[41] S. Landi, I. R. Segundo, E. Freitas, M. Vasilevskiy, J. Carneiro, C. J. Tavares, *Solid State Commun.* **2022**, *341*, 114573.
[42] S. Ghosh, A. Nakada, M. A. Springer, T. Kawaguchi, K. Suzuki, H. Kaji, I. Baburin, A. Kuc, T. Heine, H. Suzuki, R. Abe, S. Seki, *J. Am. Chem. Soc.* **2020**, *142*, 9752.
[43] Q.-Y. Wang, J. Liu, M. Cao, J.-H. Hu, R. Pang, S. Wang, M. Asad, Y.-L. Wei, S.-Q. Zang, *Angew. Chem., Int. Ed. Engl.* **2022**, *61*, 202207130.
[44] P.-F. Wei, M.-Z. Qi, Z.-P. Wang, S.-Y. Ding, W. Yu, Q. Liu, L.-K. Wang, H.-Z. Wang, W.-K. An, W. Wang, *J. Am. Chem. Soc.* **2018**, *140*, 4623.
[45] D. Chen, W. Chen, G. Zhang, S. Li, W. Chen, G. Xing, L. Chen, *ACS Catal.* **2022**, *12*, 616.
[46] T. Yanai, D. P. Tew, N. C. Handy, *Chem. Phys. Lett.* **2004**, *393*, 51.
[47] M. J. Frisch, G. W. Trucks, H. B. Schlegel, G. E. Scuseria, M. A. Robb, J. R. Cheeseman, G. Scalmani, V. Barone, G. A. Petersson, H. Nakatsuji, X. Li, M. Caricato, A. V. Marenich, J. Bloino, B. G. Janesko, R. Gomperts, B. Mennucci, H. P. Hratchian, J. V. Ortiz, A. F. Izmaylov, J. L. Sonnenberg, F. D. Williams, F. Lipparini, F. Egidi, J. Goings, B. Peng, A. Petrone, T. Henderson, D. Ranasinghe, et al., Gaussian 16 Rev. C.01, Wallingford, CT, **2016**.
[48] D. Andrae, U. Huermann, M. Dolg, H. Stoll, H. Preuʔ, *Theor. Chim. Acta* **1990**, *77*, 123.
[49] D. Roy, S. Neogi, S. De, *Process Saf. Environ. Prot.* **2022**, *161*, 723.
[50] A. Yazdanbakhsh, A. Eslami, M. Massoudinejad, M. Avazpour, *Chem. Eng. J.* **2020**, *380*, 122497.
[51] D. Zhang, B. Pan, H. Zhang, P. Ning, B. Xing, *Environ. Sci. Technol.* **2010**, *44*, 3806.
[52] J.-L. Clément, N. Ferré, D. Siri, H. Karoui, A. Rockenbauer, P. Tordo, *J. Org. Chem.* **2005**, *70*, 1198.
[53] A. Khojastegi, A. Mokhtare, I. Mosleh, A. Abbaspourrad, *Appl. Catal. A* **2022**, *646*, 118883.
[54] K. Sekar, C. Chuaicham, B. Vellaichamy, W. Li, W. Zhuang, X. Lu, B. Ohtani, K. Sasaki, *Appl. Catal. B* **2021**, *294*, 120221.
[55] M. Jahdi, S. B. Mishra, E. N. Nxumalo, S. D. Mhlanga, A. K. Mishra, *Appl. Catal. B* **2020**, *267*, 118716.